Right Ventricular Deformation Analyses Using a Three-Dimensional Speckle-Tracking Echocardiographic System Specialized for the Right Ventricle

Akiko Atsumi, MD, PhD, Yoshihiro Seo, MD, PhD, Tomoko Ishizu, MD, PhD, Akihiro Nakamura, MD, PhD, Yoshiharu Enomoto, MD, PhD, Yoshie Harimura, MD, Tomoya Okazaki, Yasuhiko Abe, and Kazutaka Aonuma, MD, PhD, *Tsukuba, Kawasaki, and Tochigi, Japan*

Background: Given the complex morphologic nature of the right ventricle, three-dimensional (3D) approaches would be more appropriate for assessing right ventricular (RV) function than two-dimensional approaches. Thus, the investigators have developed a novel 3D speckle-tracking echocardiographic (STE) system specialized for the right ventricle. The aim of this study was to assess the characteristics of RV global and regional deformation as well as changes on stress tests using the 3D STE system in experimental studies.

Methods: In 10 sheep, sonomicrometry crystals were implanted to validate 3D STE data in the RV endocardium of seven RV segments, including the basal and mid anterior, lateral and inferior wall, and outflow free wall. Full-volume 3D STE data sets and sonomicrometric data were acquired at baseline, during pulmonary artery banding (PAB)–induced moderate (peak RV pressure > 40 mm Hg) and severe (peak RV pressure > 60 mm Hg) RV pressure increases, and during propranolol infusion. The 3D STE area change ratio (ACR), longitudinal strain (LS), and circumferential strain (CS) were measured, and RV global and all segmental deformation data were compared between baseline and stress tests. To assess clinical feasibility, 30 control subjects and 11 patients with pulmonary arterial hypertension were enrolled.

Results: All combined 3D STE data were significantly correlated with the sonomicrometric data (ACR, R^2 = 0.88; LS, R^2 = 0.84; CS, R^2 = 0.82; P < .001). In all seven segments, the 3D STE data correlated with the sonomicrometric data (R^2 = 0.72–0.90, P < .001). Global ACR and LS data showed significant differences among baseline, moderate PAB, and severe PAB; however, CS differed only between baseline and severe PAB. The magnitudes of segmental deformation in the free wall were larger than those in the septum and apex under all conditions (P < .05) except LS during severe PAB. Segmental analyses also showed similar responses during stress tests; the ACR in each segment differed significantly between conditions. In all but the apical segments, LS showed significant reductions from moderate PAB; in contrast, CS was significantly reduced with severe PAB in all segments. In this clinical study, the acquisition rate of adequate images for analysis of the RV outflow tract was lower (75.6%) compared with the rate in other segments (from 85.4% to 100%). However, the pulmonary arterial hypertension group had lower RV global deformation values than the control group (ACR and LS, P < .001; CS, P = .003), the ACR and LS in basal and middle segments differed significantly between groups, and the outflow and apex did not differ.

Conclusions: A novel 3D STE system specialized for the right ventricle is reliable for RV deformation analyses and may provide additional information about RV global and segmental function. The clinical feasibility of this system is acceptable. (J Am Soc Echocardiogr 2016;■:■-■.)

Keywords: Three-dimensional echocardiography, Speckle-tracking echocardiography, Right ventricle, Cardiac function

From the Cardiovascular Division (A.A., Y.S., T.I., Y.H., K.A.), the Department of Child Health (A.N.), and the Department of Cardiovascular Surgery (Y.E.), Graduate School of Comprehensive Human Sciences, University of Tsukuba, Tsukuba, Japan; the Corporate Research and Development Center, Toshiba Corporation, Kawasaki, Japan (T.O.); and the Ultrasound Systems Division, Toshiba Medical Systems Corporation, Tochigi, Japan (Y.A.).

This work was supported by the Japan Society for the Promotion of Science KAKENHI (grant 25461041). This is an industry-related cooperative study between the University of Tsukuba and Toshiba Medical Systems Corporation (project code CGE26132). Dr Seo was supported by a research grant from Toshiba Medical Systems Corporation. Mr Okazaki is employed by Toshiba Corporation. Mr Abe is employed by Toshiba Medical Systems Corporation.

Reprint requests: Yoshihiro Seo, MD, PhD, University of Tsukuba, Cardiovascular Division, 1-1-1 Tennodai, Tsukuba 305-8575, Japan (E-mail: *yo-seo@md.tsukuba.ac.jp*).

0894-7317/$36.00

http://dx.doi.org/10.1016/j.echo.2015.12.014

Abbreviations

ACR = Area change ratio

CS = Circumferential strain

LS = Longitudinal strain

LV = Left ventricular

M-PAB = Moderate pulmonary artery banding

PAB = Pulmonary artery banding

PAH = Pulmonary arterial hypertension

RV = Right ventricular

S-PAB = Severe pulmonary artery banding

STE = Speckle-tracking echocardiographic

3D = Three-dimensional

2D = Two-dimensional

Cardiopulmonary diseases may cause right ventricular (RV) dysfunction, and in recent years, many studies have confirmed the prognostic importance of RV function.[1-6] Echocardiography is widely used to evaluate RV function using tricuspid annular plane systolic excursion and RV fractional area change.[7,8] However, assessing RV function using conventional echocardiography is difficult because of the complex nature of the RV structure and contraction in contrast to the ellipsoidal left ventricle.[9] As with the left ventricle, RV deformation imaging would provide additional information about RV pathophysiology. Two-dimensional (2D) speckle-tracking echocardiographic (STE) systems have been used to quantitate RV myocardial deformation, which could be assessed by longitudinal strain (LS) but not circumferential strain (CS), because of the complex nature of the RV structure in contrast to the ellipsoidal left ventricle.[9-11] Thus, RV global and regional deformation has not been well studied noninvasively, because an appropriate system has not yet been developed.

Given the complex nature of the right ventricle, a three-dimensional (3D) approach would be more appropriate than a 2D approach. We developed a 3D STE system for the left ventricle, and the pathophysiology and clinical feasibility of various strain components as possible imaging biomarkers were subsequently studied.[12,13] To overcome the limitation of 2D speckle-tracking echocardiography for assessing RV function, we recently reported on the preliminary use of a 3D STE system designed for left ventricular (LV) analysis and showed that 3D speckle-tracking echocardiography is useful for evaluating RV function with deformation data.[14] Similarly, Smith *et al.*[15] reported that 3D STE deformation data were associated with clinical outcomes in patients with pulmonary hypertension using the same system. However, the current 3D STE system, which is specialized for the left ventricle, may be inadequate for accurately demonstrating RV structure and function.[14,15] Thus, we developed a new 3D STE system that features a specialized algorithm for the right ventricle and sought to assess the characteristics of RV global and regional deformation with the system in experimental studies and to confirm the clinical feasibility of evaluating global and regional deformation data in normal subjects and in a small group of patients with pulmonary arterial hypertension (PAH).

METHODS

Animal Preparation

In this study, we used 10 male hybrid Suffolk sheep (Japan Lamb, Ltd, Hiroshima, Japan) weighing, on average, 27.5 kg. The study was approved by the Institutional Animal Experiment Committee of the University of Tsukuba and conducted in compliance with our university's regulations for animal experiments and the "Fundamental Guideline for Proper Conduct of Animal Experiment and Related Activities in Academic Research Institutions" of the Ministry of Education, Culture, Sports, Science and Technology.

General anesthesia was induced with thiamylal sodium (10-15 mg/kg intravenously), and endotracheal intubation was performed. Anesthesia was maintained with isoflurane (1.5%-2%) and oxygen. Two 5-F micromanometer-tipped catheters (Millar Instruments, Houston, TX) were inserted into the right ventricle via the jugular vein and into the left ventricle via the femoral artery to measure the ventricular pressure and maximal rate increase in LV pressure (dP/dt max) for each condition. Pressure data were digitized and stored on a personal computer for analysis with dedicated software. A median sternotomy was performed, and an incision was made in the pericardium avoiding the apical area.

Sonomicrometry

We implanted sonomicrometry crystals (2-mm diameter; Sonometrics Corporation, London, ON, Canada) at the RV endocardium in seven segments, including the basal and mid anterior, lateral and inferior wall, and outflow free wall. (For detailed methods, see Supplemental Figure 1.) Sonomicrometry crystals were implanted in four or five of the seven segments in each sheep, because they could not be implanted simultaneously in all segments.

Sonomicrometric data were acquired immediately after the corresponding echocardiographic images were recorded, and the data were analyzed using CardioSOFT Pro (Sonometrics Corporation). Strain was calculated as $[L(t) - L_0]/L_0$, where $L(t)$ is segment length at time t, and L_0 is segment length at the onset of the QRS complex. The LS of the basal segment was measured between the basal and mid endocardial crystals, whereas the LS of the mid segment was measured between the mid and apical endocardial crystals. The CS of the basal and mid segments was measured between each endocardial crystal pair. The area change ratio (ACR) was calculated using a function in CardioSOFT that can multiply two sonomicrometric curves. The ACR was calculated with a longitudinal and circumferential curve of each segment.[12,13] All strain data were calculated by averaging data from 10 consecutive heartbeats. Any curves that were not recorded clearly were excluded from the analysis.

Echocardiography

Echocardiographic examinations were performed with an ARTIDA ultrasonography system (Toshiba Medical Systems, Tochigi, Japan). Full-volume electrocardiography-gated 3D data sets with six sectors were acquired in the apical position using a matrix-array 2.5-MHz transducer. In each study, the heart was repositioned within the apical pericardium to control for apical motion. A peritoneal incision was made to acquire the appropriate 3D apical images through the diaphragm. The animal's breathing was stopped during the image acquisition process. The volume rate of each image was set at 30 to 40 Hz. The data were stored and transferred to a computer (Inspiron 1300; Dell, Inc, Round Rock, TX) for offline analysis. The images were analyzed with prototype software for the right ventricle.

We used a 3-MHz transducer for conventional echocardiography. LV volume and ejection fraction were measured using the modified Simpson's rule.[16] RV diameter and function were determined with RV diameter (length, papillary muscle, and basal level), fractional area change, tricuspid annular plane systolic excursion, and peak systolic velocity of the tricuspid annulus using the tissue Doppler method.

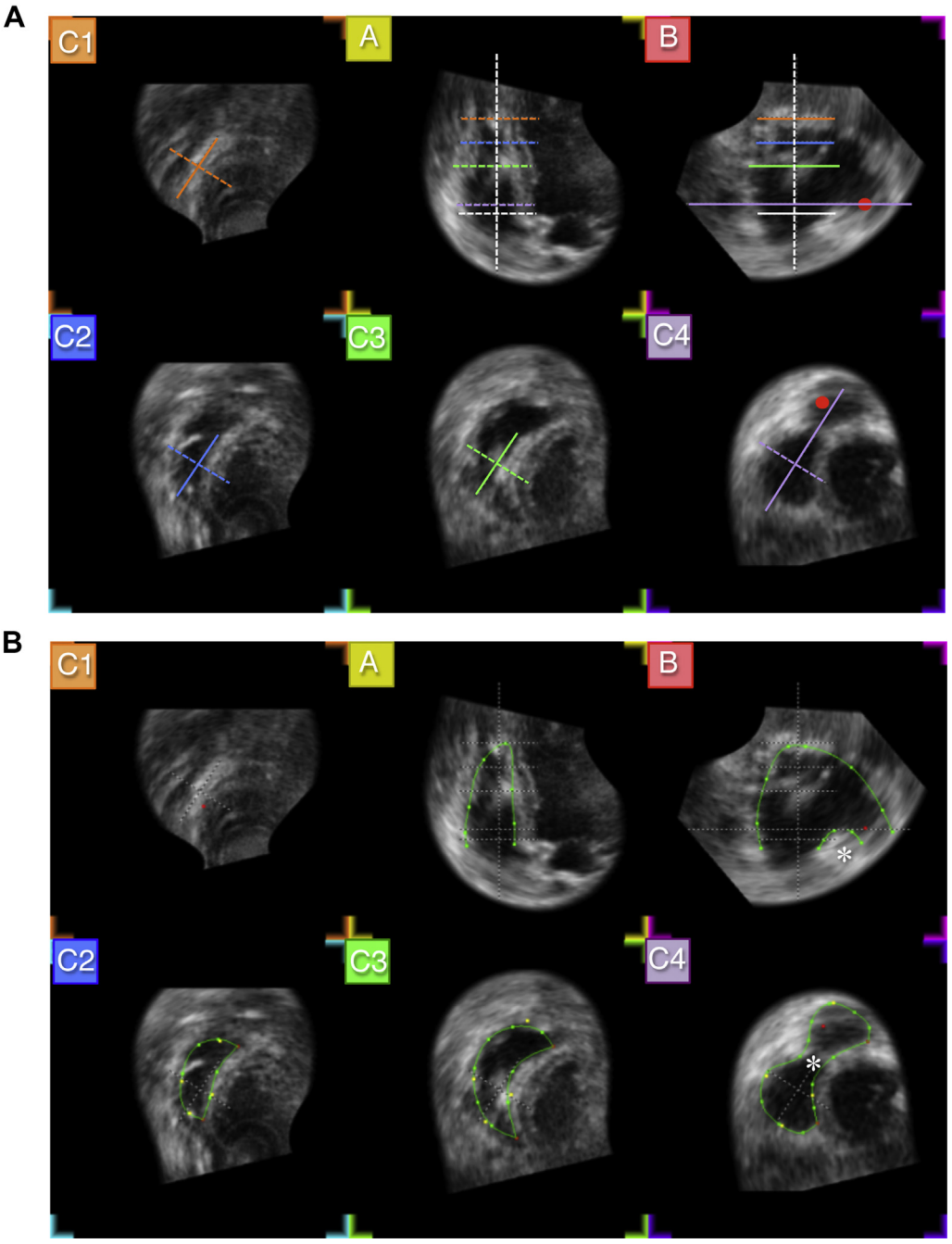

Figure 1 Three-dimensional speckle-tracking echocardiography of the right ventricle. The multiplanar reconstruction images at end-diastole correspond to the apical four-chamber view **(A)**, sagittal plane **(B)**, and four short-axis views at different levels **(C1–C4)**, which are used as the reference images to determine the tracking points. The top panel indicates the method used to determine the reference images and the positional correlations. Both the long-axis views **(A,B)** are at right angles to each other along a common longitudinal axis (*white dotted vertical line*). Of the four orthogonal short-axis views, **C1** indicates an apical point, a point at the intersection of the *orange dotted line* in **A** with the *orange solid line* in **B**. **C2** indicates an apical short-axis view at the level including the *blue dotted line* in **A** and the *blue solid line* in **B**. Similarly, **C3** indicates an RV mid-short-axis view at the level including the *green dotted line* in **A** and the *green solid line* in **B**. Finally, **C4** indicates an RV short-axis view crossing the RV outflow, which is shown as a *red point*, at the level including the *purple dotted line* in **A** and a *purple solid line* in **B**. The bottom horizontal *white dotted line* in **A** and the *white solid line* in **B** show the tricuspid valve level. In the bottom panel, the green lines show traced RV endocardial contours and the points used to determine the trace contours, which must be manually set on the images. *The "-" marker in **B** and **C4** indicates the ventriculoinfundibular fold.

Three-Dimensional Wall Motion Tracking Algorithm

First, the tracking points were distributed on the 3D curved surfaces of the RV myocardium at the end of the diastolic phase, which were estimated by traced lines on multiplanar reconstruction images (Figure 1). In the template-matching process, the template volume in the current frame was generated from an approximately

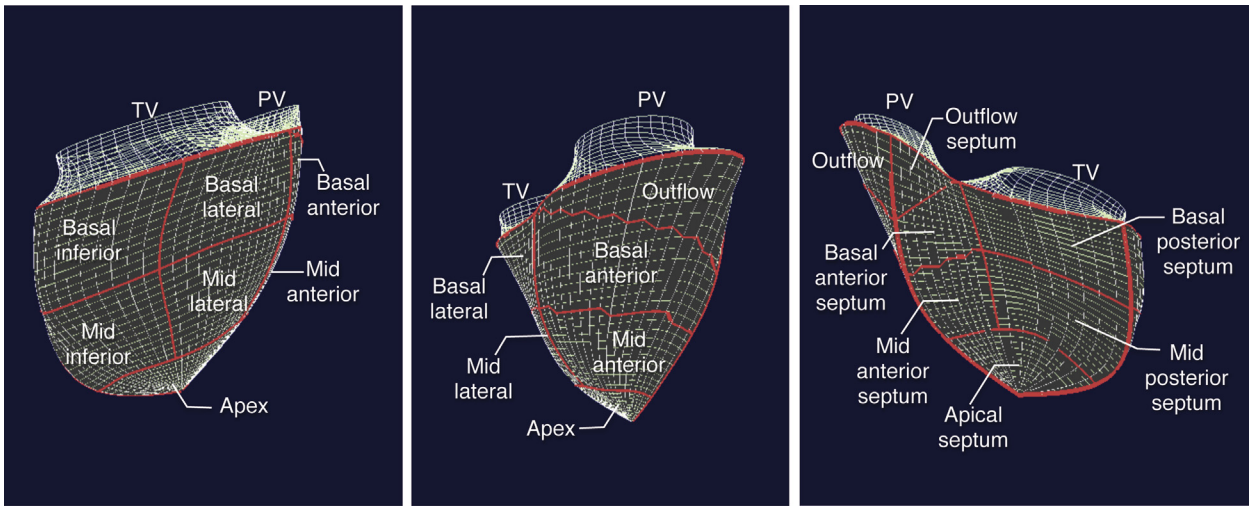

Figure 2 Fourteen segments of the right ventricle. The left panel shows the free wall viewed from the inferior side. The middle panel shows the free wall and outflow viewed from the anterior side. The right panel shows the septum wall of the right ventricle. *PV*, Pulmonary valve; *TV*, tricuspid valve.

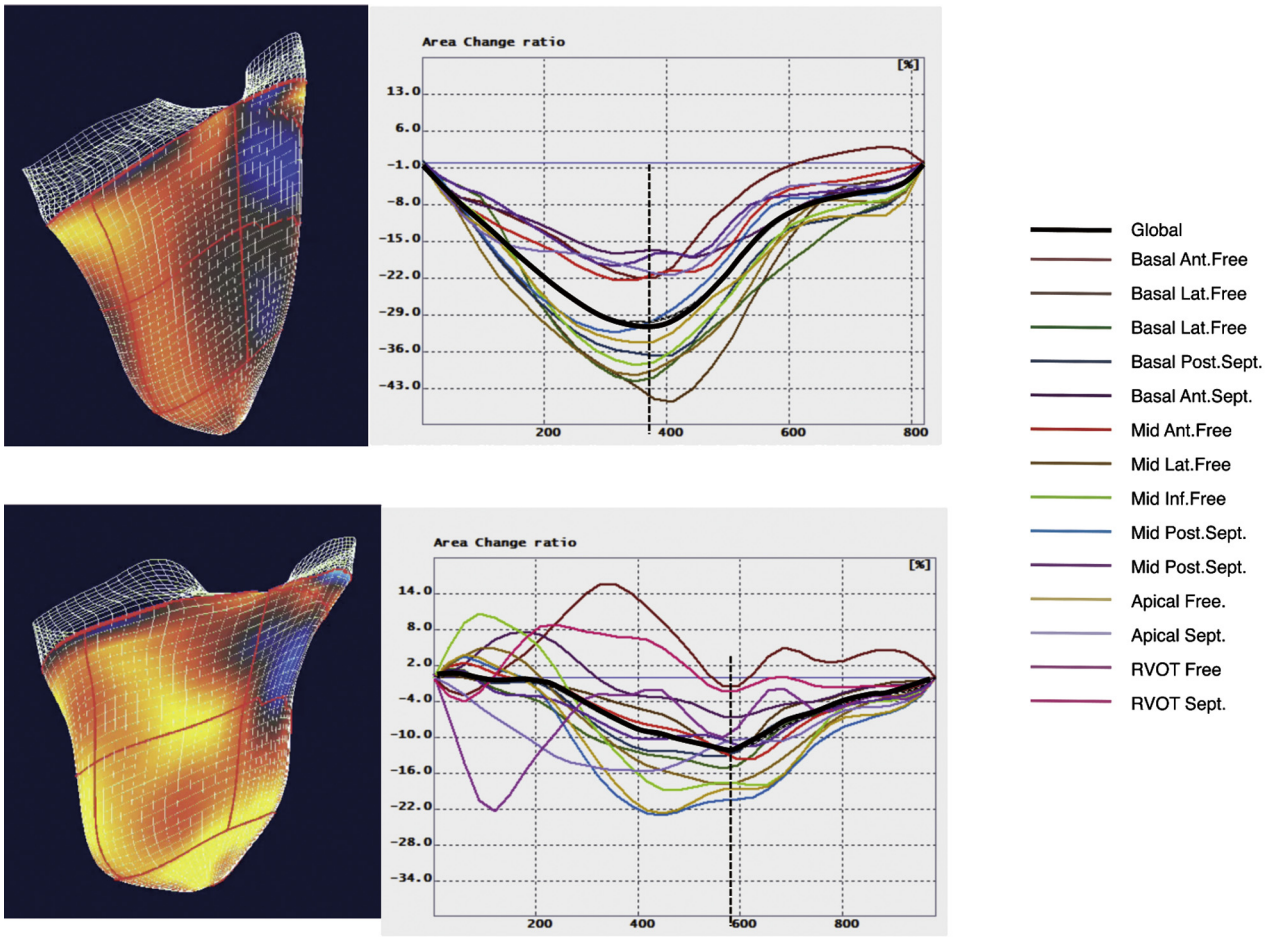

Figure 3 Strain profiles in a representative case. The top panels depict baseline global and segmental strain-time curves. The bottom panels depict global and segmental strain-time curves during S-PAB. Each vertical broken line shows the surrogate point to measure deformation data corresponding to the maximum deformation point of the global deformation data.

$10 \times 10 \times 10$ mm cube.[12] The most similar point in the next volume was found by the comparison of a template volume with the cube in the next volume. We used the 3D sum of squared differences method to test image similarity. Finally, the motion vectors were interpolated using a 3D interpolation algorithm. After these steps, arbitrary points of interest on the cardiac wall could be tracked by integrating the

Table 1 Hemodynamic and 2D echocardiographic parameters

Variable	Baseline	M-PAB	S-PAB	*P* value, ANOVA	Propranolol infusion	*P* value, base vs propranolol infusion
HR (beats/min)	110.4 ± 3.4	109.8 ± 5.2	105.2 ± 5.0*†	<.001	92.8 ± 5.6	.001
LVSP (mm Hg)	82.3 ± 9.0	76.6 ± 9.0	50.6 ± 9.0*†	<.001	60.8 ± 9.0	.004
LV dP/dt	2,050 ± 223	1,597 ± 268	1,031 ± 196*†	<.001	1,183 ± 178	.001
RVSP (mm Hg)	22.1 ± 2.9	47.4 ± 3.4*	63.2 ± 2.2*†	<.001	22.1 ± 2.4	.99
RV dP/dt	679.8 ± 46.2	542.2 ± 36.6*	449.7 ± 52.4*†	<.001	350.3 ± 35.2	<.001
LVEDV (mL)	26.6 ± 4.8	24.7 ± 4.6	15.7 ± 4.2*†	.004	28.1 ± 5.0	.71
LVESV (mL)	6.8 ± 2.0	5.9 ± 1.8	3.7 ± 1.9*	<.001	9.8 ± 1.8	.10
LVEF (%)	75.6 ± 3.9	77.0 ± 4.3	77.6 ± 4.2	<.001	65.3 ± 4.2	.01
RV-long (mm)	42.3 ± 3.3	40.1 ± 3.6	46.3 ± 3.8*†	.045	42.8 ± 3.4	.81
RV-PM (mm)	17.9 ± 2.2	16.9 ± 2.3	23.8 ± 2.8*†	.001	19.5 ± 2.1	.88
RV-base (mm)	22.7 ± 2.5	23.1 ± 2.5	26.1 ± 2.6*	.02	25.5 ± 2.1	.13
FAC (%)	63.2 ± 9.0	54.4 ± 8.9	40.7 ± 8.3*†	.23	52.4 ± 10.1	.07
TAPSE (mm)	8.8 ± 0.9	7.2 ± 1.5	5.2 ± 0.9*†	.001	7.0 ± 1.2	.03
TA S′ (cm/sec)	10.4 ± 1.4	7.5 ± 1.8*	4.7 ± 1.4*	<.001	6.7 ± 1.4	.03

ANOVA, Analysis of variance; *FAC*, fractional area change; *HR*, heart rate; *LVEDV*, LV end-diastolic volume; *LVEF*, LV ejection fraction; *LVESV*, LV end-systolic volume; *LVSP*, LV systolic pressure; *RV-base*, basal RV dimension; *RV-long*, RV dimension of longitudinal axis; *RV-PM*, RV dimension at papillary muscle level; *RVSP*, RV systolic pressure; *TAPSE*, tricuspid annular plane systolic excursion; *TA S′*, tricuspid annular systolic velocity. Data are expressed as mean ± 95% CI. *P* value ANOVA is the overall *P* value from the mixed-model analysis.
*$P < .05$ versus baseline.
†$P < .05$ versus M-PAB.

interpolated motion vectors over all frames during a single cardiac cycle. We visually identified tracking quality according to the tracking quality of the endocardial trace line on the multiplanar reconstruction images. The 3D RV images were then automatically obtained and divided into a total of 14 segments, including five basal, five middle, two apical, and two RV outflow (Figure 2). All strain data were measured on a single heartbeat. The temporal changes in the strain data were displayed as a color-coded "plastic bag" image as well as time-strain curves including global and segmental RV strain (Figure 3). The surrogate point used to measure deformation data was set at the minimum point (maximum deformation point) of the global deformation data on the strain-time curve (Figure 3).

Experimental Protocol

After the baseline measurements were recorded, partial ligations of the main pulmonary artery were performed to increase RV afterload in two stages. The first stage caused moderately increased afterload (moderate pulmonary artery banding [M-PAB]), such that RV systolic pressure increased by ≥40 mm Hg. The 3D echocardiographic and sonomicrometric data during M-PAB were recorded about 5 min after pulmonary artery banding (PAB) to obtain data during stable condition. After a 10-min rest period, we confirmed that hemodynamics and RV function recovered to the baseline. Then, RV systolic pressure increased to ≥60 mm Hg, leading to severely increased afterload (severe PAB [S-PAB]). The data acquisitions during S-PAB were performed immediately after RV pressure exceeded 60 mm Hg, as hemodynamic collapse would occur in a few minutes. After a 10-min rest period, we confirmed that hemodynamics and RV function recovered to the pre–propranolol infusion test baseline. Next, a continuous infusion of propranolol (4-8 μg/kg/min) was initiated to reduce contractility. The infusion dose was increased and maintained until the RV dP/dt max had decreased by ≥25% compared with that at baseline. The 3D echocardiographic and sonomicrometric data were recorded during the steady administration of propranolol.

Reproducibility

All the baseline data were used to assess intra- and interobserver reproducibility. To test intraobserver variability, a single observer analyzed the data on two occasions with a 1-month interval. To test interobserver variability, a second observer analyzed the data without knowledge of the first observer's measurements. Reproducibility was assessed using the mean absolute percentage error (absolute difference divided by the mean of the two observations).

Clinical Studies

The 3D and 2D echocardiographic examinations were performed in the same setting as the experimental studies. Thirty normal subjects and 11 patients with PAH were enrolled. Normal subjects were healthy volunteers, while patients with PAH were previously diagnosed according to current guidelines.[17] Subjects with atrial fibrillation or frequent premature beats were excluded. We assessed the acquisition rate of adequate images by confirming clearly defined endocardial contours in each segment as well as 3D STE parameters for comparing normal subjects and patients with PAH. The study was approved by an institutional review committee, and all subjects provided informed consent.

Statistical Analysis

Data are shown as mean ± 95% CI. The data were statistically analyzed using linear regression and Bland-Altman analysis to determine the bias and limits of agreement between the modalities. A mixed-model analysis was used to compare results among variables at baseline and during M-PAB and S-PAB. When significant intergroup

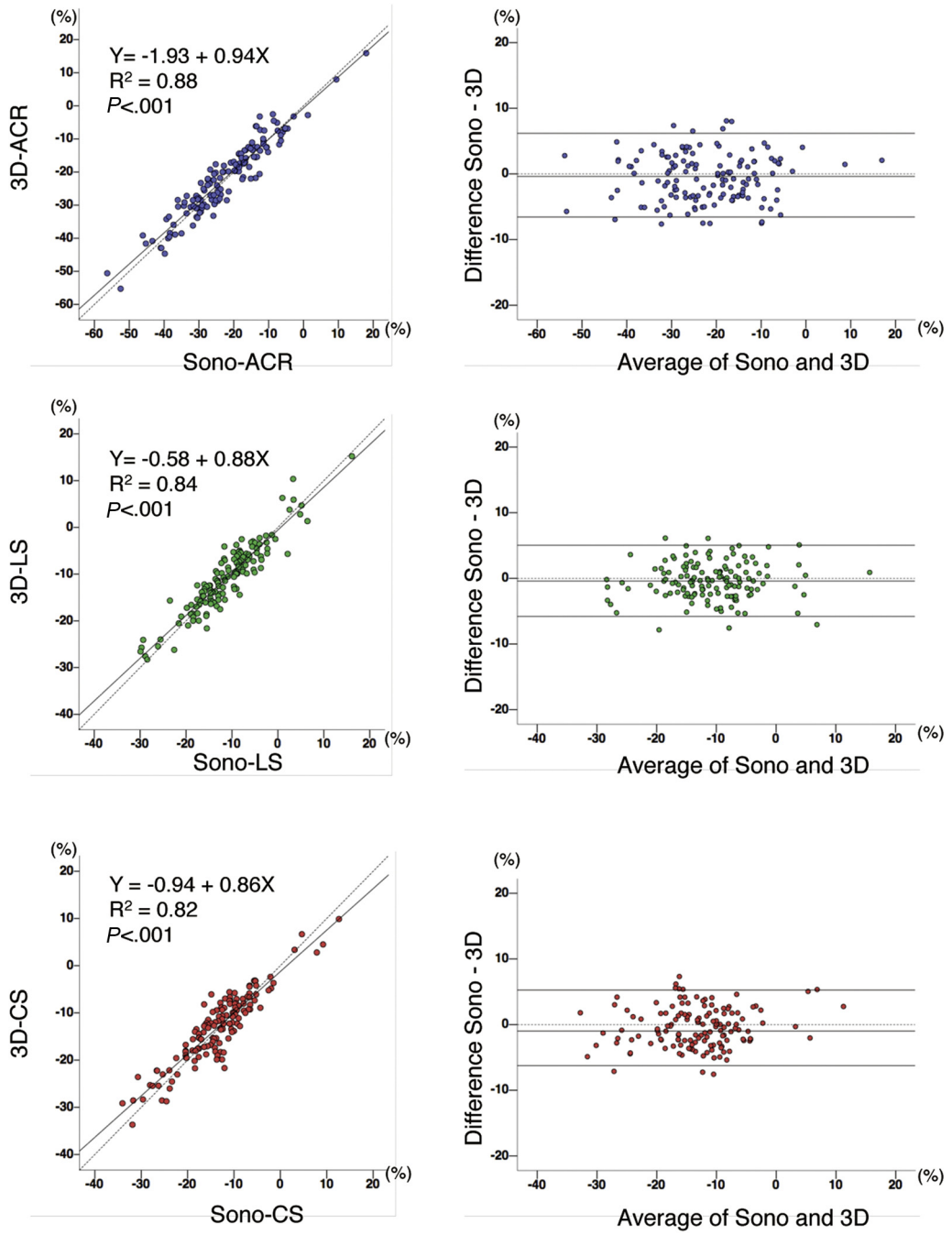

Figure 4 Correlations between deformation data using 3D speckle-tracking echocardiography and sonomicrometry (Sono). The left panel shows a correlation diagram, while the right panel shows a Bland-Altman plot for each strain. The top figure shows data of the ACR, the middle figure shows data of LS, and the bottom figure shows data of CS. The *solid lines* in the left panel are regression lines for all measurements, while the *dotted lines* show $Y = X$. The *solid lines* in the right panel show the mean differences and the 95% limits of agreement.

differences were present, a Bonferroni test was performed to compare individual groups. A paired *t* test was used to compare the baseline and propranolol infusion results. In addition, mixed-model analyses were performed to determine the differences among segments at same condition.

P values $< .05$ were considered to indicate statistical significance. We used SPSS version 22 for Mac (SPSS, Inc, Chicago, IL) for the statistical analyses.

RESULTS

Table 1 summarizes the hemodynamic and conventional echocardiographic data. RV systolic pressure ranged from 41.6 to 56.4 mm Hg during M-PAB and from 60.2 to 69.8 mm Hg during S-PAB. During propranolol infusion, RV dP/dt max was significantly reduced compared with baseline (changes in RV dP/dt; range, −29.1% to −63.6%). RV dimensions increased and LV volume decreased during

Table 2 Correlation of each segment between 3D STE method and sonomicrometry

	Basal			Mid			
Variable	Anterior	Lateral	Inferior	Anterior	Lateral	Inferior	Outflow
ACR	0.88	0.81	0.90	0.86	0.85	0.90	0.88
LS	0.88	0.86	0.79	0.82	0.81	0.90	0.83
CS	0.86	0.72	0.85	0.81	0.79	0.77	0.86

All results were statistically significant ($P < .001$).

S-PAB. Fractional area change and tricuspid annular plane systolic excursion were reduced during S-PAB compared with baseline and M-PAB; however, they did not differ between baseline and M-PAB. Peak systolic velocity of the tricuspid annulus was reduced in each stress test compared with baseline; however, it did not differ between M-PAB and S-PAB.

Three-Dimensional Speckle-Tracking Echocardiography versus Sonomicrometry

One hundred twenty data sets were available for analysis of the correlation of strain data between sonomicrometry and 3D speckle-tracking echocardiography. Figure 4 shows the correlations between sonomicrometry and the 3D STE data. Each parameter was strongly correlated between the two methods. In the Bland-Altman plots, the fixed bias and 95% limits of agreement were −0.38% and −6.56% to 6.18% for the ACR, −0.77% and −5.67% to 4.90% for LS, and −0.98% and −6.24% to 5.26% for CS, respectively. In each segment, the 3D STE data were significantly correlated with the sonomicrometric data (Table 2).

Changes in RV STE Data Induced by Stress Tests

A representative case is shown in Figure 3, showing the dramatic changes to the RV strain profile induced by S-PAB. The magnitudes of RV global ACR and LS during M-PAB and S-PAB were significantly lower than those at baseline (Figure 5). For a detailed description of the changes in 3D STE RV segmental deformation data by stress tests, see Supplemental Figure 2.

Reproducibility

Intra- and interobserver reproducibility was 6.9% and 7.7%, respectively, for the ACR measurements; 8.6% and 11.1%, respectively, for the LS measurements; and 6.0% and 8.6%, respectively, for the CS measurements.

Clinical Study

Table 3 shows the baseline characteristics and echocardiographic data. The number (proportion) of cases for which 3D echocardiographic image quality was suitable for speckle-tracking analysis was low in the outflow segments at 31 cases (75.6%) in the outflow free wall and outflow septum (Table 4). In the remaining segments, the lowest rate of feasibility was observed in the mid anterior wall in the control group (83.3%). The magnitude of global strain was significantly lower in the PAH group than in the normal control group (ACR, −26.7 ± 4.0% vs −12.2 ± 3.3%, $P < .001$; LS, −12.2 ± 3.3% vs −5.8 ± 3.0%, $P < .001$; CS, −10.1 ± 3.6% vs −4.6 ± 2.4%, $P < .001$). In all the basal and mid segments, the magnitudes of ACR, LS, and CS in the PAH group were significantly lower than those in the control group. No significant differences in apical and outflow free wall segments were common to all of the deformation data.

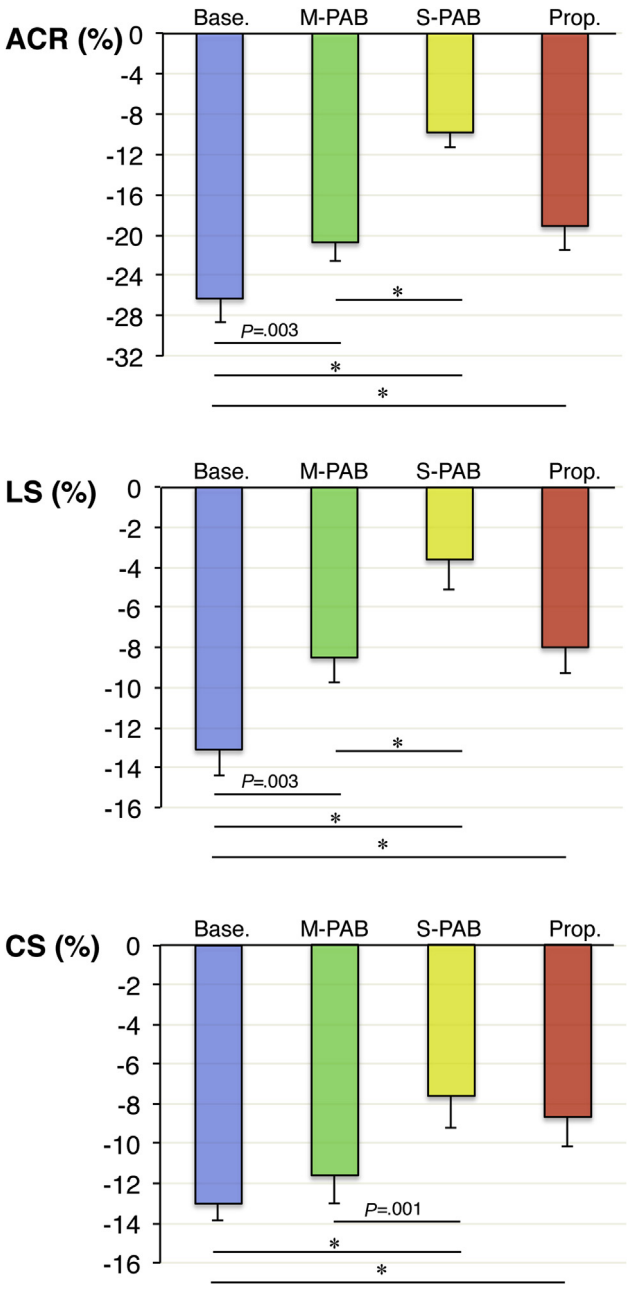

Figure 5 Changes in global deformation on stress tests. The top figure shows data of the ACR, the middle figure shows data of LS, and the lower figure shows data of CS. Each parameter between baseline (Base.), during M-PAB, and during S-PAB are compared. Data during propranolol infusion (Prop.) were compared with baseline. Data are shown as mean ± 95% CI. *$P < .001$.

DISCUSSION

This is the first study to report on a 3D STE system designed specifically to assess RV function. Using experimental animal studies, we demonstrated the reliability and clinical feasibility of a novel 3D STE system for the right ventricle. The following characteristics of

Table 3 Comparisons of baseline characteristics and 2D echocardiographic parameters between normal subjects and patients with PAH

Variable	Normal (n = 30)	PAH (n = 11)	P
Age (y)	49.1 ± 17.2	47.0 ± 13.5	.74
Sex (male)	18 (60%)	4 (36.4%)	.49
BSA (m^2)	1.58 ± 0.16	1.51 ± 0.16	.77
SBP (mm Hg)	124.8 ± 17.2	118.1 ± 16.0	.19
DBP (mm Hg)	71.1 ± 16.4	71.8 ± 10.3	.91
HR (beats/min)	66.1 ± 11.6	81.5 ± 14.6	.01
RVSP by echocardiography (mm Hg)	22.9 ± 5.5 (n = 27)	83.5 ± 36.1	<.001
LVEDV (mL)	73.0 ± 17.2	48.2 ± 20.3	.001
LVESV (mL)	23.9 ± 6.4	13.8 ± 13.8	.01
LVEF (%)	66.8 ± 6.1	73.1 ± 5.2	.004
RV-long (mm)	62.8 ± 9.2	77.7 ± 8.4	<.0001
RV-PM (mm)	28.1 ± 5.2	40.7 ± 8.1	<.0001
RV-base (mm)	31.3 ± 5.4	44.8 ± 8.5	<.0001
FAC (%)	48.9 ± 4.2	27.9 ± 7.8	<.0001
TAPSE (mm)	21.0 ± 2.3	15.5 ± 3.7	.001
TA S′ (cm/sec)	13.3 ± 1.7	10.3 ± 2.2	.003

BSA, Body surface area; *DBP*, diastolic blood pressure; *SBP*, systolic blood pressure. Other abbreviations as in Table 1.
Data are expressed as mean ± SD or number (percentage).

RV deformation were revealed. Heterogeneous magnitudes of segmental deformation were present in the right ventricle. Responses of RV global and segmental deformation during PAB differed between LS and CS; LS was more sensitive to pressure overload. The clinical study confirmed that 3D STE data acquisitions are feasible in the clinical setting; however, the 3D STE system is less effective in the outflow segments.

Advantages

We previously reported a preliminary study for RV function analyses with 3D speckle-tracking echocardiography; however, detailed regional function could not be assessed because the LV 3D STE system was diverted to the right ventricle.[14] Therefore, we developed a novel system specifically for RV regional and global function analyses. This novel 3D STE system traces the ventricular surface to determine the tracking points. In the complex right ventricle, determining the correct orientation points enabled adequate tracing with better reproducibility. The system uses a RV surface model that is reconstructed using three parts, including the RV body (free wall and septum) and the inflow and outflow tracts. As shown in Supplemental Figure 1, relatively complex methods are necessary to trace the RV surface; however, this process allows us to accurately reconstruct a 3D RV surface.

Reliability

The quantification of regional RV function is challenging; however, such data may be useful in various cardiac diseases. Myocardial strain measurement has been a focus for assessing segmental myocardial function since speckle-tracking echocardiography became commercially available.[18,19] In previous validation studies for 2D and 3D STE measurements, strain data measured by sonomicrometry were considered the gold standard; therefore, we selected sonomicrometry to validate deformation data obtained using the 3D STE system.[12,13,18,19] Because of the limitations of the sonomicrometric method, deformation in the septum and apex cannot be assessed; however, the strong correlation of each deformation variable between 3D speckle-tracking echocardiography and sonomicrometry in all analyzed segments demonstrated that the 3D STE system is reliable for assessing regional deformation. In addition, the 95% limits of agreements from Bland-Altman plots were acceptable and support the 3D STE system's reliability. Furthermore, the reproducibility of each deformation variable was considered acceptable because a limit of <10% variability was used as a feasible cutoff level for measurements in previous echocardiographic studies.[20] The current manual tracing method used to determine surfaces of the RV myocardium may be a major cause of this variability. In the future, the development of automatic border detection systems would contribute to improved measurement variability.

Response to Stress Tests

PAB and the propranolol infusion changed RV function. During PAB, the magnitude of global ACR and LS gradually decreased depending on banding level severity. However, global CS during M-PAB did not significantly decrease compared with baseline CS. During M-PAB, RV structure did not change, despite significant increases in pulmonary artery pressure. Accordingly, pressure overload resulted mainly in changes in the ACR and LS but not in CS, which suggests that longitudinal contraction may be more sensitive for pressure overload. The disturbances between LS and CS may be due to the two-layer structure of the RV myocardium; the endocardial layer has longitudinal myofibers, whereas the epicardial layer has circumferential myofibers.[9] The epicardial fiber is continuous with the LV myocardium; therefore, circumferential contraction may depend on LV contraction even during pressure overload.

The longitudinal fiber direction is damaged first in the left ventricle because the endocardial fiber direction is longitudinally oriented.[21,22] Therefore, in the right ventricle also during pressure overload, endocardial muscle dysfunction may occur before epicardial muscle impairment. Compared with that in the left ventricle, longitudinal shortening disturbances in the right ventricle may undergo subendocardial damage because the longitudinal fiber layer lies only in the endocardium in the right ventricle, whereas this layer lies in both the endocardium and epicardium in the left ventricle. During S-PAB, remarkable RV structural changes occur that can change fiber direction and increase wall stress, thus deteriorating the circumferential contraction.

Segmental Analysis

Our baseline data revealed intraventricular deformation heterogeneity in that the deformation in the free wall was greater than that in the septal and apical segments. The intersegment differences in the deformation data were more remarkable in the ACR and CS compared with that in the LS. The heterogeneity in each strain component may reflect the underlying mechanics of RV contraction. These findings suggest that the primary functional direction of the right ventricle is longitudinal and that the relative strength of the deformation would depend on circumferential contraction. The segmental variability may be associated with distinctive RV movements. The continuity of the

Table 4 Comparisons of regional deformation data by 3D speckle-tracking echocardiography between normal subjects and patients with PAH

	ACR			LS			CS		
Segment	Control (n = 30)	PAH (n = 11)	P	Control	PAH	P	Control	PAH	P
Basal anterior	−29.6 ± 9.4 (29)	−9.1 ± 5.0 (10)	<.001	−17.0 ± 7.8	−3.1 ± 4.2	<.001	−9.1 ± 6.2	−1.5 ± 5.4	.005
Basal lateral	−40.2 ± 9.6 (29)	−20.3 ± 9.1 (11)	<.001	−20.1 ± 9.9	−9.7 ± 4.1	.001	−15.7 ± 8.7	−9.2 ± 6.1	.01
Basal inferior	−43.1 ± 8.0 (29)	−26.2 ± 7.4 (11)	<.001	−15.8 ± 7.7	−10.4 ± 4.6	.01	−29.3 ± 6.7	−17.6 ± 5.9	<.001
Basal PS	−33.6 ± 8.6 (30)	−20.7 ± 8.4 (11)	<.001	−13.9 ± 6.8	−8.4 ± 6.7	.03	−19.5 ± 7.6	−12.9 ± 3.4	.001
Basal AS	−23.0 ± 8.8 (28)	−8.8 ± 3.5 (10)	<.001	−15.9 ± 6.7	−5.0 ± 4.5	<.001	−6.3 ± 5.7	−0.4 ± 5.7	.03
Mid anterior	−17.5 ± 7.6 (25)	−4.4 ± 5.6 (10)	.001	−9.4 ± 6.5	−2.3 ± 7.8	.01	−9.6 ± 7.0	−2.4 ± 6.6	.01
Mid lateral	−27.8 ± 9.8 (27)	−12.1 ± 6.2 (11)	<.001	−14.5 ± 8.3	−6.6 ± 6.8	.01	−12.5 ± 8.2	−6.9 ± 4.0	.01
Mid inferior	−37.7 ± 6.2 (29)	−23.3 ± 9.1 (11)	<.001	−18.5 ± 6.2	−10.8 ± 6.7	.002	−21.4 ± 5.7	−14.2 ± 6.2	.002
Mid PS	−29.9 ± 6.3 (30)	−19.9 ± 4.6 (11)	<.001	−14.3 ± 6.1	−8.8 ± 3.7	.009	−15.5 ± 5.3	−12.4 ± 3.7	.04
Mid AS	−19.8 ± 7.2 (27)	−13.7 ± 4.8 (11)	.002	−11.3 ± 5.1	−4.8 ± 5.1	.003	−7.8 ± 3.4	−2.1 ± 4.7	.02
Apical FW	−24.8 ± 7.9 (29)	−20.7 ± 9.1 (11)	.19	−9.0 ± 3.5	−8.4 ± 3.6	.73	−9.5 ± 5.8	−7.9 ± 5.1	.41
Apical septal	−19.8 ± 6.4 (28)	−13.7 ± 4.6 (11)	.007	−8.2 ± 2.3	−5.3 ± 1.7	.01	−6.2 ± 3.0	−4.7 ± 2.2	.10
OT FW	−21.5 ± 9.0 (22)	−16.9 ± 9.5 (9)	.30	−10.8 ± 6.2	−7.5 ± 9.1	.50	−8.9 ± 5.5	−5.0 ± 9.3	.21
OT septal	−19.0 ± 7.2 (22)	−11.1 ± 9.8 (9)	.04	−10.8 ± 7.4	−7.6 ± 9.7	.21	−6.8 ± 4.0	−5.5 ± 3.7	.49

AS, Anterior septum; *FW*, free wall; *OT*, outflow; *PS*, posterior septum.
Data are expressed as mean ± SD. A case number with adequate images to assess deformation data in each segment is in parentheses.

muscle fibers between the left and right ventricles functionally binds both and represents the anatomic basis of RV free wall contraction caused by LV contraction.[9] Therefore, RV free wall contraction may be greater than that in other regions.

Changes in segmental deformation data by stress tests were similar to those of global deformation.

Because the ACR differed between stress conditions in almost all the segments, it may be a more robust parameter for detecting regional contraction abnormalities.

Clinical Feasibility

As expected, our system was able to reveal the significant differences in global deformation data between normal patients and those with PAH. With regard to regional deformation analyses, there were no significant differences in deformation data between normal subjects and patients with PAH in the outflow segments. The results would be due to the low feasibility of image acquisitions in the outflow segment. The acquisition of adequate images in the outflow segments is a challenge for 3D speckle-tracking echocardiography, as the RV outflow is located behind the sternum, which is outside the transthoracic echocardiographic window. In addition, the lung may have been positioned between the RV outflow and the echocardiographic probe. In our segmentations of the 3D STE system, the RV outflow segments were small and located just below the pulmonary valve (Figures 1 and 2). On the basis of the anatomic definition, the basal to mid anterior segments might be classified as part of the RV outflow. Because the feasibility in the basal to mid anterior segments was acceptable, the outflow segmentations require future reconsideration to improve clinical feasibility.

Study Limitations

In this study, sonomicrometry crystals were implanted only in the basal and mid free wall because the septal wall and apical area were too small to allow sufficient crystal implantation. Each study was performed at a relatively high heart rate. The low frame rate of 3D speckle-tracking echocardiography could cause an incorrect interframe correlation and may possibly have affected tracking quality and strain data. Interobserver reproducibility was slightly high, whereas intraobserver reproducibility was <10%. The high variability may affect the results of strain changes in various conditions or segmental strain values; therefore, further efforts are necessary to reduce variability and reveal the actual deformation of the RV regional wall.

In the present study, we used the open-chest sheep model, in which ventricular coupling and septal deformation, during PAB in particular, could have been affected by the open pericardium. Therefore, strain data may differ from those under closed chest conditions.

The clinical study did not have a cohort design; therefore, the prognostic predictable value of each variable was uncertain. Future prospective cohort studies are necessary to identify the clinical impact of each variable.

CONCLUSIONS

This novel 3D STE system specialized for the right ventricle is reliable for RV global and segmental function analyses, as it revealed the characteristics of the right ventricle, heterogeneity of magnitude of segmental deformation, and different responses against acute pressure overload between longitudinal and circumferential components. These findings could provide additional information about RV global and segmental functional analyses and may contribute to the identification of novel RV pathophysiology. Additionally, its feasibility was confirmed as acceptable in the clinical setting.

REFERENCES

1. Kjaergaard J, Akkan D, Iversen KK, Kober L, Torp-Pedersen C, Hassager C. Right ventricular dysfunction as an independent predictor of short- and

long-term mortality in patients with heart failure. Eur J Heart Fail 2007;9:610-6.
2. Meyer P, Filippatos GS, Ahmed MI, Iskandrian AE, Bittner V, Perry GJ, et al. Effects of right ventricular ejection fraction on outcomes in chronic systolic heart failure. Circulation 2010;121:252-8.
3. Ghio S, Klersy C, Magrini G, D'Armini AM, Scelsi L, Raineri C, et al. PrognoSTEc relevance of the echocardiographic assessment of right ventricular function in patients with idiopathic pulmonary arterial hypertension. Int J Cardiol 2010;140:272-8.
4. Swift AJ, Rajaram S, Campbell MJ, Hurdman J, Thomas S, Capener D, et al. PrognoSTEc value of cardiovascular magnetic resonance imaging measurements corrected for age and sex in idiopathic pulmonary arterial hypertension. Circ Cardiovasc Imaging 2014;7:100-6.
5. Haddad F, Doyle R, Murphy DJ, Hunt SA. Right ventricular function in cardiovascular disease, part II: pathophysiology, clinical importance, and management of right ventricular failure. Circulation 2008;117:1717-31.
6. van Wolferen SA, Marcus JT, Boonstra A, Marques KM, Bronzwaer JG, Spreeuwenberg MD, et al. Prognostic value of right ventricular mass, volume, and function in idiopathic pulmonary arterial hypertension. Eur Heart J 2007;28:1250-7.
7. Miller D, Farah MG, Liner A, Fox K, Schluchter M, Hoit BD. The relation between quantitative right ventricular ejection fraction and indices of tricuspid annular motion and myocardial performance. J Am Soc Echocardiogr 2004;17:443-7.
8. Lopez-Candales A, Dohi K, Rajagopalan N, Edelman K, Gulyasy B, Bazaz R. Defining normal variables of right ventricular size and function in pulmonary hypertension: An echocardiographic study. Postgrad Med J 2008;84:40-5.
9. Haddad F, Hunt SA, Rosenthal DN, Murphy DJ. Right ventricular function in cardiovascular disease, part I: anatomy, physiology, aging, and functional assessment of the right ventricle. Circulation 2008;117:1436-48.
10. Fukuda Y, Tanaka H, Sugiyama D, Ryo K, Onishi T, Fukuya H, et al. Utility of right ventricular free wall speckle-tracking strain for evaluation of right ventricular performance in patients with pulmonary hypertension. J Am Soc Echocardiogr 2011;24:1101-8.
11. Motoji Y, Tanaka H, Fukuda Y, Ryo K, Emoto N, Kawai H, et al. Efficacy of right ventricular free-wall longitudinal speckle-tracking strain for predicting long-term outcome in patients with pulmonary hypertension. Circ J 2013;77:756-63.
12. Seo Y, Ishizu T, Enomoto Y, Sugimori H, Yamamoto M, Machino T, et al. Validation of 3-dimensional speckle tracking imaging to quantify regional myocardial deformation. Circ Cardiovasc Imaging 2009;2:451-9.
13. Seo Y, Ishizu T, Enomoto Y, Sugimori H, Aonuma K. Endocardial surface area tracking for assessment of regional lv wall deformation with 3d speckle tracking imaging. JACC Cardiovasc Imaging 2011;4:358-65.
14. Atsumi A, Ishizu T, Kameda Y, Yamamoto M, Harimura Y, Machino-Ohtsuka T, et al. Application of 3-dimensional speckle tracking imaging to the assessment of right ventricular regional deformation. Circ J 2013;77:1760-8.
15. Smith BC, Dobson G, Dawson D, Charalampopoulos A, Grapsa J, Nihoyannopoulos P. Three-dimensional speckle tracking of the right ventricle: toward optimal quantification of right ventricular dysfunction in pulmonary hypertension. J Am Coll Cardiol 2014;64:41-51.
16. Lang RM, Badano LP, Mor-Avi V, Afilalo J, Armstrong A, Ernande L, et al. Recommendations for cardiac chamber quantification by echocardiography in adults: an update from the American Society of Echocardiography and the European Association of Cardiovascular imaging. J Am Soc Echocardiogr 2015;28:1-39. e14.
17. Hoeper MM, Bogaard HJ, Condliffe R, Frantz R, Khanna D, Kurzyna M, et al. Definitions and diagnosis of pulmonary hypertension. J Am Coll Cardiol 2013;62(25 Suppl):D42-50.
18. Leitman M, Lysyansky P, Sidenko S, Shir V, Peleg E, Binenbaum M, et al. Two-dimensional strain-a novel software for real-time quantitative echocardiographic assessment of myocardial function. J Am Soc Echocardiogr 2004;17:1021-9.
19. Amundsen BH, Helle-Valle T, Edvardsen T, Torp H, Crosby J, Lyseggen E, et al. Noninvasive myocardial strain measurement by speckle tracking echocardiography: aalidation against sonomicrometry and tagged magnetic resonance imaging. J Am Coll Cardiol 2006;47:789-93.
20. Gottdiener JS, Bednarz J, Devereux R, Gardin J, Klein A, Manning WJ, et al. American society of echocardiography recommendations for use of echocardiography in clinical trials. J Am Soc Echocardiogr 2004;17:1086-119.
21. Gallagher KP, Stirling MC, Choy M, Szpunar CA, Gerren RA, Botham MJ, et al. Dissociation between epicardial and transmural function during acute myocardial ischemia. Circulation 1985;71:1279-91.
22. Cheng A, Nguyen TC, Malinowski M, Daughters GT, Miller DC, Ingels NB Jr. Heterogeneity of left ventricular wall thickening mechanisms. Circulation 2008;118:713-21.

Appendix

Supplemental Material

Changes in Segmental Deformation Data Determined Using Stress Tests. Changes in 3D STE RV segmental deformation data by stress tests. The magnitudes of segmental deformation in the free wall were larger than those in the septum and apex under all conditions ($P < .05$) except for LS during S-PAB.

In each segment, significant changes of ACR were observed with PAB (Supplemental Figure 2A). In particular, significant differences were observed among baseline, M-PAB, and S-PAB. The propranolol infusion reduced the ACR in all segments compared with baseline.

In all but the apical segments, LS was reduced even during M-PAB compared with baseline (Supplemental Figure 2B). LS in the basal and mid anterior wall, basal posteroseptum, and outflow free wall was reduced to a level that did not differ from LS during S-PAB.

In contrast, significant changes in CS were not observed during M-PAB and were observed compared with baseline in all segments during S-PAB only (Supplemental Figure 2C). Propranolol infusion reduced both LS and CS in almost all segments compared with baseline data.

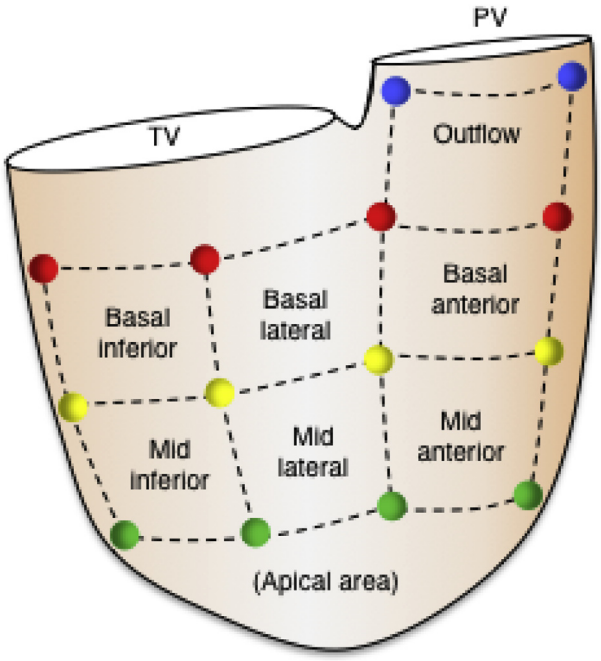

Supplemental Figure 1 Schematic of the implanted positions of the sonomicrometry crystals on the RV free wall. *Red dots* show basal crystal position; *yellow ones*, mid; *green ones*, apical; and *blue ones*, outflow. We implanted the sonomicrometry crystals in a square shape on all seven segments (basal anterior, mid anterior, basal lateral, mid lateral, basal inferior, mid inferior, and outflow). *PV*, Pulmonary valve; *TV*, tricuspid valve.

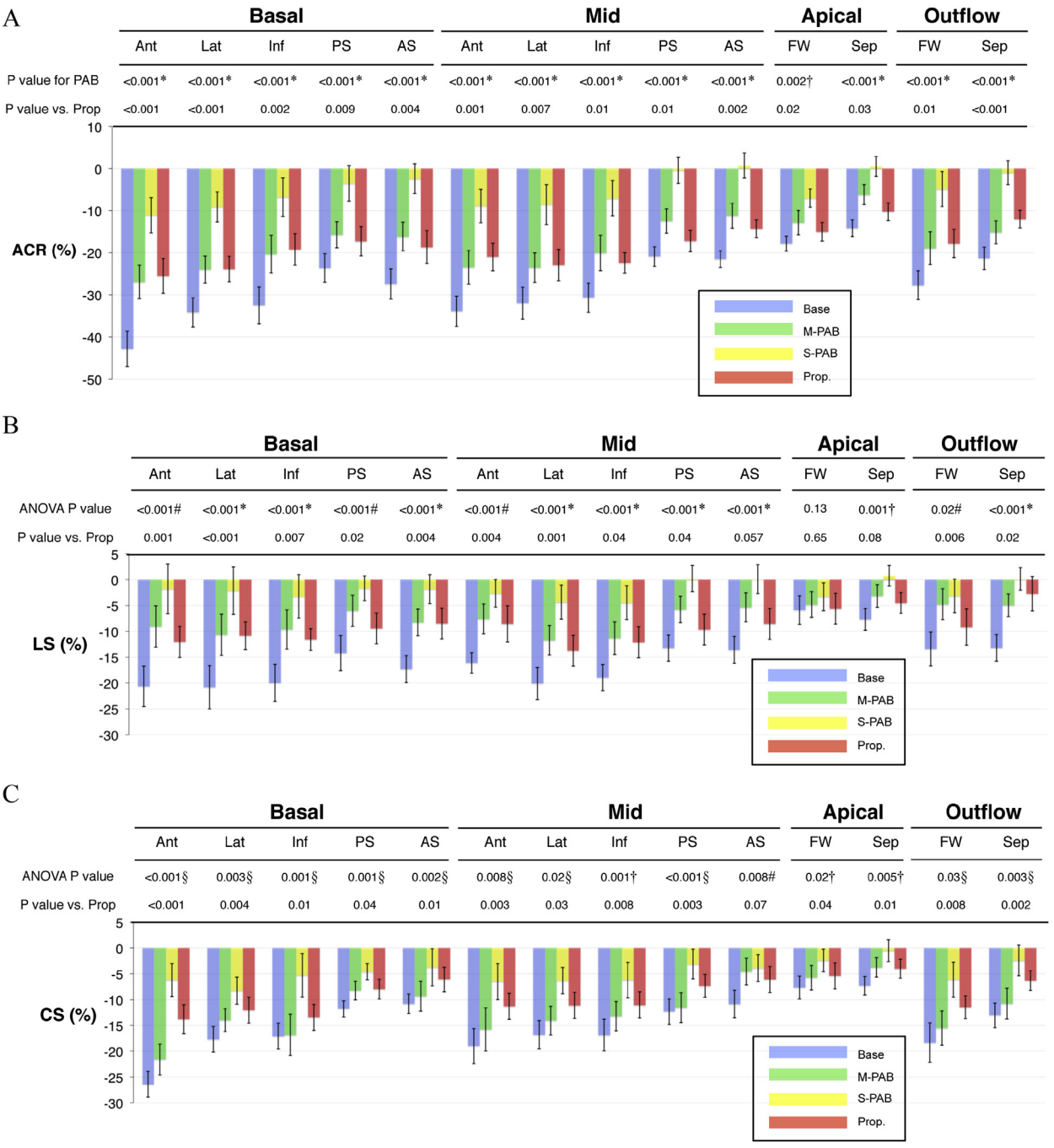

Supplemental Figure 2 **(A)** ACR, **(B)** LS, and **(C)** CS. Blue bars indicate RV 14-segment data at baseline, green ones indicate data during M-PAB, yellow ones indicate data during S-PAB, and orange ones indicate data during propranolol infusion. Data are shown as mean ± 95% CI. *Ant*, Anterior; *AS*, anterior septum; *FW*, free wall; *Inf*, inferior; *Lat*, lateral; *Prop.*, propranolol; *PS*, posterior septum; *Sep*, septum. *P* value for PAB is the overall *P* value from the mixed-model analysis compared with baseline, M-PAB, and S-PAB in each segment. *P* value versus propranolol infusion is the *P* value from a paired *t* test in the comparison between baseline and propranolol infusion in each segment. The following significant differences were derived from the comparisons in the same segment: $^{*}P < 0.05$ between baseline, M-PAB, and S-PAB; $^{\dagger}P < .05$, baseline versus S-PAB; $^{\#}P < .05$, baseline versus both M-PAB and S-PAB; $^{\S}P < .05$, S-PAB versus both baseline and M-PAB.